

1 Authors' version.

2 Published in:

3 IEEE TRANSACTIONS ON BIOMEDICAL ENGINEERING, VOL. 55, NO. 7, JULY 2008

4 Digital Object Identifier 10.1109/TBME.2008.919842

5

6

7 Valentina Agostini<sup>1</sup>, Silvia Delsanto<sup>1</sup>, Marco Knaflitz<sup>1</sup>, *Member, IEEE* and Filippo Molinari<sup>1</sup>, *Member,*

8

*IEEE*

9

<sup>1</sup>Dip. Elettronica, Politecnico di Torino, Corso Duca degli Abruzzi 24, 10129 Torino, Italy

10

11 **Noise estimation in infrared image sequences: a tool for the**  
12 **quantitative evaluation of the effectiveness of registration**  
13 **algorithms**

14

15

16 *Abstract* — Dynamic infrared imaging has been proposed in literature as an adjunctive technique to  
17 mammography in breast cancer diagnosis. It is based on the acquisition of hundreds of consecutive  
18 thermal images with a frame rate ranging from 50 frames/s to 200 frames/s, followed by the harmonic  
19 analysis of temperature time series at each image pixel. However, the temperature fluctuation due to  
20 blood perfusion, which is the signal of interest, is small compared to the signal fluctuation due to subject  
21 movements. Hence, before extracting the time series describing temperature fluctuations, it is  
22 fundamental to realign the thermal images to attenuate motion artifacts. In this paper, we describe a  
23 method for the quantitative evaluation of any kind of feature-based registration algorithm on thermal  
24 image sequences, provided that an estimation of local velocities of reference points on the skin is  
25 available. As an example of evaluation of a registration algorithm, we report the evaluation of the signal  
26 to noise ratio improvement obtained by applying a non-rigid piecewise linear algorithm.

27

28 *Index Terms*—Dynamic infrared imaging, image registration, signal-to-noise ratio estimation, thermal  
29 image sequence, breast cancer detection.

30

## I. INTRODUCTION

31 Currently, the screening gold standard in breast cancer diagnosis is mammography. Since the early  
32 seventies, thermography has been proposed as a possible adjunct to mammography in screening, but static  
33 thermography - i.e., the simple measurement of breast skin temperature - yielded no satisfactory results  
34 [1]. More recently, Dynamic Area Telethermometry (DAT) [2-3], also known as Dynamic InfraRed  
35 Imaging (DIRI) [4-5], has been proposed as a new imaging modality for breast cancer detection. It  
36 requires the acquisition of a sequence of hundreds of consecutive thermal images with a rate ranging from  
37 50 frames/s to 200 frames/s. The harmonic analysis of the time course of temperature fluctuations allows  
38 to obtain information on the local blood perfusion. In literature, it has been reported that temperature  
39 fluctuations have an important diagnostic value in oncology [2-3]. In fact, recent studies have  
40 demonstrated that cancer-associated extra vascular nitric oxide determines a perturbation in the normal  
41 modulation of the local blood flow, which can be detected through the analysis of the fluctuations of  
42 temperature at each sample region [2-5]. Hence, after subdividing the region of interest in square sub-  
43 regions (approximately 4 mm<sup>2</sup> each) consisting of one or more pixels, spectral analysis of the temperature  
44 time series corresponding to each sub-region is performed.

45 In our experimental protocol, the acquisition of the image sequence lasts 10 seconds, during which  
46 the patient's breast moves non-rigidly due to physiological (breathing, heart activity, ...) and random  
47 movements. Consequently, the signal of interest, i.e., the small temperature fluctuations due to  
48 perturbations of the blood perfusion in a certain region, is superimposed to signal fluctuations arising  
49 from the subject motion. This is because temperature samples corresponding to different skin regions are  
50 recorded as belonging to the same region observed by the infrared sensor. Motion artifacts are then  
51 particularly relevant in areas in which a strong spatial gradient of temperature is present.

52 Therefore, before proceeding with the harmonic analysis of the temperature time series in each square  
 53 sub-region, it is fundamental to properly realign the thermal images composing the sequence to attenuate  
 54 motion artifacts. Although some Authors have reported the detrimental effect of motion artifacts [4], at  
 55 this time there is no quantitative evaluation of the power due to the effects of motion artifacts with respect  
 56 to that of the signal of interest. This also limits the possibility of objectively evaluating the performance  
 57 of different algorithms for realigning infrared sequences [6].

58 The goal of this paper is to propose a method to quantitatively evaluate the performances of marker-  
 59 based registration algorithms in dynamic infrared imaging, in terms of improvement of the signal to noise  
 60 ratio. This approach can be applied to any kind of registration algorithm based on control points, provided  
 61 that an estimation of local image velocities is available. We then present the results obtained by applying  
 62 the proposed approach to evaluate the improvement of the signal to noise ratio obtained through a  
 63 piecewise linear registration algorithm applied to sequences relative to three subjects with different breast  
 64 size.

## 65 II. MATERIALS AND METHODS

### 66 A. The model

67 First, we introduce a model for the noise estimation in dynamic infrared imaging. Considering a small  
 68 portion of skin and indicating by  $T(x,y,t)$  the temperature that the infrared sensor measures in the point  
 69  $(x,y)$  at a given time instant  $t$ , temperature variations in time captured by the infrared camera are a  
 70 combination of the physiological variations of the skin temperature (the signal of interest) and of apparent  
 71 temperature changes actually due to patient's movements (noise).

72 The total derivative of temperature with respect to time,  $dT/dt$ , is:

73

$$\begin{aligned}
 \frac{dT}{dt} &= \frac{\partial T}{\partial t} + \frac{\partial T}{\partial x} \frac{\partial x}{\partial t} + \frac{\partial T}{\partial y} \frac{\partial y}{\partial t} = \\
 &= \frac{\partial T}{\partial t} + (\vec{v} \cdot \nabla)T
 \end{aligned}
 \tag{1}$$

74

75 where  $\vec{v} = (v_x, v_y)$  is the 2-dimensional velocity of the skin portion and  $\nabla T$  is the spatial temperature  
 76 gradient. Equation 2 reports the expression of the noise  $N(x, y, t)$  introduced by motion artifacts.

$$77 \quad N(x, y, t) \approx \int_0^t \vec{v}(x, y, t') \cdot \nabla T(x, y, t') dt' \quad (2)$$

78 A measure of the performance of a realignment algorithm applied to the infrared image sequence is the  
 79 improvement of the signal-to-noise ratio obtained through the registration. The signal-to-noise ratio of the  
 80 process - at each point  $(x, y)$  - is defined as  $S/N \equiv \sigma_T^2(x, y) / \sigma_N^2(x, y) - 1$ , where  $\sigma_T^2(x, y)$  is the  
 81 variance of the measured temperature time series  $T(x, y, t)$  (signal plus noise) and  $\sigma_N^2(x, y)$  is the variance  
 82 of the noise, as given by Eq. (2). Similarly, we define the signal-to-noise ratio after registration as  
 83  $(S/N)_R \equiv \sigma_{T_R}^2(x, y) / \sigma_{N_R}^2(x, y) - 1$ , where  $\sigma_{T_R}^2(x, y)$  is the variance of the measured temperature time  
 84 series  $T_R(x, y, t)$  obtained after sequence realignment and  $\sigma_{N_R}^2(x, y)$  is the variance of the  
 85 term  $\int_0^t \vec{v}_R(x, y, t') \cdot \nabla T_R(x, y, t') dt'$ , being  $\vec{v}_R(x, y, t)$  the residual velocity, not compensated by the  
 86 registration algorithm.

### 87 *B. Acquisition system and patient positioning*

88 The infrared image sequences were acquired with an AIM256Q camera (Long Wave Quantum Well  
 89 Infrared Photodetector, 256×256 pixels, produced by AEG Infrarot-Module GmbH, Germany). The  
 90 acquisition time was equal to 10 seconds and the frame rate was 50 frames/s; hence, each sequence  
 91 consisted of 500 thermal images of 256×256 pixels.

92 The sensor noise declared by the constructor of the infrared camera is equal to 17.3 mK (given as  
 93 NETD, with an integration time of 20 ms) and thus is negligible compared to noise due to patient's  
 94 movement, estimated by simulations, which is typically of the order of hundreds of mK. Hence, in our  
 95 model, we considered the patient's movement as the only noise source.

96 The patient was asked to lie down onto an examination table with a backrest inclination of 40 degrees

97 with respect to the horizontal plane. She was also asked to raise up her arms with the hands resting over  
 98 her head. We acquired a frontal view comprehending both breasts.

99 Before the acquisition, two sets of wooden spherical markers (5 mm in diameter) were applied to the  
 100 skin to obtain a) control points, i.e. contrasted features for registration, and b) test points, for evaluating  
 101 the goodness of the registration itself. In particular, as control points we placed 6-8 equally spaced  
 102 markers around each breast contour, one roughly at the center of the previous ones, and 2 on the sternum.  
 103 Test points consisted of markers applied internally to each breast contour. All markers were fixed to the  
 104 skin by means of biocompatible glue. Figure 1a shows a typical placement of control points (light-colored  
 105 markers) and of test points (dark markers).

### 106 III. IMAGE REGISTRATION AND REGISTRATION EVALUATION

#### 107 A. *Image Registration*

108 The first step in any feature-based registration is the detection of the control points that are used to  
 109 compute the transformation. To localize control and test points, we developed a specific algorithm for the  
 110 automatic segmentation of the image and labeling of markers [6].

111 Centroids of control points were used to obtain a piece-wise linear transformation based on a Delaunay  
 112 triangulation [7] of the region to be registered. Figure 1b shows an example of triangulation. We chose  
 113 this specific transformation because it is reported to give good results when small geometric differences  
 114 between the images to be registered are expected [8], as in this case.

115 Here we reported the specific registration algorithm we adopted only for the sake of completeness, but  
 116 we emphasize that the signal-to-noise ratio estimation method we propose can be applied to any kind of  
 117 registration algorithm based on control points, if an estimation of local image velocities is available.

#### 118 B. *Registration Evaluation*

119 In order to evaluate the signal-to-noise ratio before and after the registration, we estimated the velocities  
 120  $\vec{v}$  and  $\vec{v}_R$ . We tested, on the three subjects that were included in this paper, different algorithms to

121 interpolate the velocities, both in the registered and in the non-registered sequences. We benchmarked the  
 122 results using Nearest-Neighbors (NN), Linear Interpolation (LI), and Biharmonic Spline Interpolation  
 123 (SI), for estimating the velocities within the region of interest. Results, in terms of SNR quantification,  
 124 were different from subject to subject: for subject 1 (small breast size) LI was better than the others, for  
 125 subject 3 (large breast size) NN was the best, and for subject 2 (medium breast size) all the techniques  
 126 behaved similarly. Specifically, considering the three interpolation techniques applied to subject 2  
 127 (medium breast size) in terms of SNR increment due to registration no statistical significance was found  
 128 (Student's t-test,  $P > 0.05$ ). Presently, our results do not show any significant difference among the  
 129 techniques we tested. We chose NN since we believe it gives acceptable results in most of the tested  
 130 conditions and for the majority of the subjects (medium breast size). To this purpose, we calculated the  
 131 Voronoi regions [9] associated to test marker centroids (see Fig. 1c) and assumed that the points  
 132 belonging to the same Voronoi region had equal velocity.

133 The instantaneous velocity  $\vec{v}$  of a certain marker centroid  $(x_t, y_t)$  at time  $t$  was calculated using a two-  
 134 point forward approximation:

$$135 \quad v_{x,t} = \frac{x_{t+1} - x_t}{\Delta t}; v_{y,t} = \frac{y_{t+1} - y_t}{\Delta t},$$

136 where  $\Delta t = 20$  ms is the sampling period.

137 The image gradient is computed using the digital approximation of the first order derivative in its anti-  
 138 symmetrical and linear implementation, i.e. by convolving the image with the vector  $[-0.5 \ 0 \ 0.5]$ .

#### 139 IV. UNCERTAINTY IN SNR CALCULATION

140 The SNR depends on velocities and temperature gradients as stated by Eq. 2. In this Section we show  
 141 how the localization error affects the SNR estimation and we provide a worst-case estimate of the  
 142 uncertainty.

143 The uncertainty on the SNR may be expressed by the uncertainty on the noise computed according to  
 144 Eq. 2, in which  $\vec{v}$  and  $\nabla T$  are independent variables. Let  $u(x)$  and  $u(y)$  be respectively the uncertainty

145 on the localization of marker centroids along  $x$  and  $y$ . The uncertainty on the noise value is expressed by  
 146 Eq. 3.

$$147 \quad u(N(x, y, t)) = \sqrt{\left( \frac{\partial \int_0^t \vec{v}(x, y, t') \cdot \nabla T(x, y, t') dt'}{\partial x} u(x) \right)^2 + \left( \frac{\partial \int_0^t \vec{v}(x, y, t') \cdot \nabla T(x, y, t') dt'}{\partial y} u(y) \right)^2} \quad (3)$$

148 By applying the partial derivative operator on the first term of Eq. 3 we obtain Eq. 4, in which, by  
 149 assuming the tissue as locally inextensible ( $\frac{\partial \vec{v}(x, y, t')}{\partial x} = 0$ ), we can neglect the first term.

$$150 \quad \frac{\partial \int_0^t \vec{v}(x, y, t') \cdot \nabla T(x, y, t') dt'}{\partial x} = \int_0^t \left[ \frac{\partial \vec{v}(x, y, t')}{\partial x} \cdot \nabla T(x, y, t') + \vec{v}(x, y, t') \cdot \frac{\partial \nabla T(x, y, t')}{\partial x} \right] dt' \quad (4)$$

151 The second term of Eq. 3 may be treated similarly. Assuming that the behavior along  $x$  and  $y$  is similar,  
 152 the two terms of Eq. 3 may be considered as equal. It follows that

$$153 \quad u(N(x, y, t)) = \sqrt{2 \cdot \left[ \int_0^t \vec{v} \cdot \frac{\partial \nabla T}{\partial x} dt' \right]^2 \cdot [u(x)]^2} \cong \sqrt{2 \cdot \left[ \frac{\Delta x}{\Delta t} \cdot \frac{\partial \nabla T}{\partial x} \cdot \Delta t \right]^2 \cdot [u(x)]^2} \quad (5)$$

154 Posing  $\Delta x = 0.1 \text{ px}$ ,  $\frac{\partial \nabla T}{\partial x} = 0.25 \text{ K} \cdot \text{px}^{-2}$ ,  $u(x) = 0.015 \text{ px}$  (values obtained from our database of images  
 155 using a 8-time oversampling [6]), we obtain a value of noise uncertainty of the order of 0.5 mK. After  
 156 realignment with a piecewise linear algorithm we have a residual error approximately equal to 20 mK,  
 157 and hence forty times larger than noise uncertainty. Hence, the uncertainty on the SNR value is  
 158 approximately 0.25 dB.

159 In order to test the dependence of the proposed SNR measure on the accuracy of the calculated  
 160 velocities we performed a robustness analysis considering different registration transformations:  
 161 PieceWise Linear (PWL), Polynomial of order 4 (P4), and Linear Conformal (LC), i.e., a transformation  
 162 that can include a rigid roto-translation, and/or a scaling. The uncertainty on the localization of marker  
 163 centroids ranges from 0.015 to 0.022 px for the three registration transformations. The corresponding

164 uncertainty on the measure of the SNR is less than 0.4 dB in the worst case.

## 165 V. RESULTS

166 The three subjects whose results are reported in this paper had respectively small breast size (cup A,  
167 subject 1), medium breast size (cup B, subject 2), and large breast size (cup DD, subject 3).

168 Fig. 1a shows the two sets of markers applied to subject 3 (large breast size), whereas Fig. 1b depicts a  
169 thermographic shot of the same subject showing superimposed (black lines) the Delaunay triangulation  
170 used in the registration procedure.

171 Figure 2 summarizes the results relative to these subjects. For each subject we report some parameters  
172 describing the signal-to-noise ratio relative to the Region Of Interest (ROI) before and after applying the  
173 registration algorithm. Specifically, we report the values of the median, 25<sup>th</sup> and 75<sup>th</sup> percentiles,  
174 minimum and maximum of the signal-to-noise ratios expressed in decibels. The ROI is defined as the area  
175 contained within the perimeter constituted by the outer triangulation lines. Notice that this ROI is slightly  
176 changing over time. However, given the small percentage of pixels entering/exiting the ROI with respect  
177 to the minimum-area ROI (less than 2 %), we decided to discard these pixels and to consider the same  
178 ROI for all the frames of the sequence.

179 Considering the three subjects above described, before registration, the signal-to-noise ratio median  
180 ranged from 1 to 2 dB (thin line boxes), whereas, after registration, it increased up to 9 dB, thus  
181 demonstrating that registration causes a decrement of the noise power due to motion artifact as high as 5-  
182 6 times, depending on the subject.

## 183 VI. CONCLUSION

184 In this paper, we present a methodology to estimate the noise due to patient motion that affects an  
185 infrared image sequence. In turns, the knowledge of noise power allows to estimate the signal-to-noise  
186 ratio that characterizes the sequence.

187 Results herein presented demonstrate that, as long as the assumptions on which the noise model is



188 based hold, it is possible to compute the signal-to-noise ratio of a specific infrared sequence of images.  
189 This is an original and important result, since it allows to assess objectively the effectiveness of different  
190 registration algorithms, as well as to obtain a quantitative evaluation of the quality of an infrared sequence  
191 of images.

192 The evaluation of the ROC curves of any detector used to differentiate sequences obtained from normal  
193 or pathological subjects is not possible without the knowledge of the signal-to-noise ratio of the sequence.  
194 Hence, we believe this noise estimation method will crucial to fill a gap that currently limits the  
195 possibility of further improving the results given by dynamic infrared imaging in early breast cancer  
196 detection and, consequently, also limits its spreading in clinics.

#### 197 ACKNOWLEDGMENT

198 This work was supported by the Fondazione CRT (Torino, Italy) in the research framework of the  
199 Clinical Industrial Research Park Foundation (Torino, Italy).

#### 200 REFERENCES

- 201 [1] K.R. Foster, "Thermographic detection of breast cancer", *IEEE Eng. Med. Biol.*, Vol. 17, Issue 6, pp.  
202 10-14, 1998.
- 203 [2] M. Anbar, L. Milesco, A. Naumov, C. Brown, T. Button, C. Carty and K. AlDulaimi, "Detection of  
204 Cancerous Breasts by Dynamic Area Telethermometry", *IEEE Eng. Med. Biol.*, Vol. 20, pp. 80-91,  
205 2001.
- 206 [3] M. Anbar, C. Brown, L. Milesco, L. Babalola and L. Gentner, "The potential of dynamic area  
207 telethermometry in assessing breast cancer", *IEEE Eng. Med. Biol.*, Vol. 19, pp. 58-62, Mar./Apr.  
208 2000.
- 209 [4] T.M. Button, H. Li, P. Fisher, R. Rosenblatt, K. Dulaimy, S. Li, B. O'Hea, M. Salvitti, V. Geronimo,  
210 C. Geronimo, S. Jambawalikar, P. Carvelli and R. Weiss, "Dynamic infrared imaging for the  
211 detection of malignancy", *Phys. Med. Biol.*, 49, pp. 3105-3116, 2004.

- 212 [5] M. Janicek, G. Demetri, M.R. Janicek, K. Shaffer, M.A. Fauci, “Dynamic Infrared Imaging of Newly  
213 Diagnosed Malignant Lymphoma Compared with Gallium-67 and Fluorine-18 Fluorodeoxyglucose  
214 (FDG) Positron Emission Tomography”, *Tech. In Cancer Res. and Treatment*, Vol. 2, Num. 6, pp.  
215 571-577, 2003.
- 216 [6] V. Agostini, S. Delsanto, F. Molinari, M. Knaflitz, “Evaluation of feature-based registration in  
217 dynamic infrared imaging for breast cancer diagnosis”, Proceedings of the 28<sup>th</sup> IEEE EMBS Annual  
218 International Conference, New York, USA, pp.953-956, 2006.
- 219 [7] A. Goshtasby, “Piecewise linear mapping functions for image registration”, *Pattern Recognition*, vol.  
220 19, pp. 459-466, 1986.
- 221 [8] L. Zagorchev, and A. Goshtashby, “A Comparative Study of Transformation Functions for Nonrigid  
222 Image Registration”, *IEEE Transactions on Image Processing*, vol. 15, no. 3, pp. 529-538, 2006.
- 223 [9] F. Aurenhammer, Voronoi diagrams—a survey of a fundamental geometric data structure, *ACM*  
224 *Computing Surveys (CSUR)*, vol. 23, Issue 3, pp. 345 – 405, 1991.
- 225

226

227 **Figures captions**

228 Fig. 1a. Picture of subject 3. Control points are represented by light-colored markers, while test points by  
229 dark markers. Fig. 1b-c. Single frame extracted from the infrared sequence: Delaunay triangulation is  
230 shown superimposed (Fig. 1b); Voronoi regions are shown superimposed (Fig. 1c).

231

232

233 Fig. 2. Boxplot of the signal to noise ratio (SNR) before (thin line) and after (thick line) registration for  
234 three different subjects respectively with small (subject 1), medium (subject 2) and large (subject 3) breast  
235 size. Each box reports the median value, percentiles (25<sup>th</sup> and 75<sup>th</sup>), minimum and maximum representing  
236 the SNR(x,y) distribution relative to the region of interest.

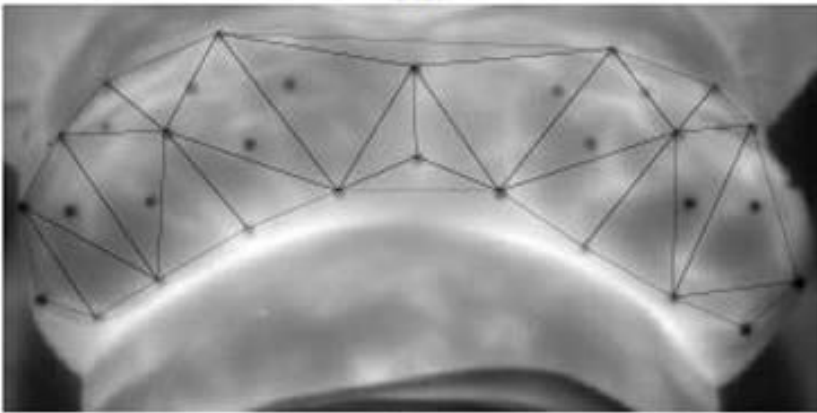
237

238 Figura 1

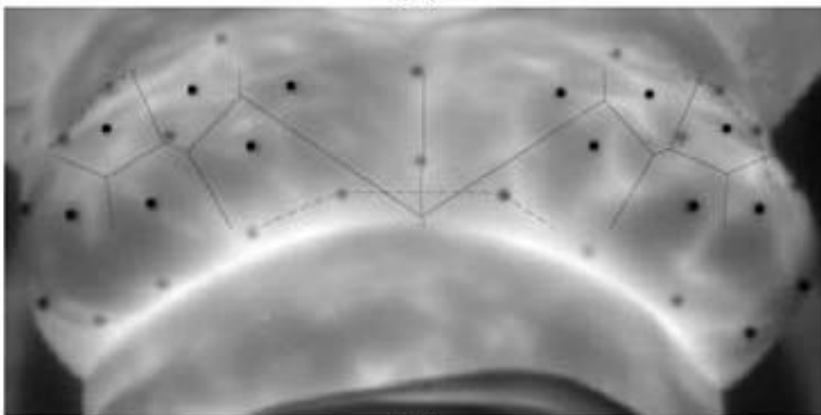
239



(a)



(b)



(c)

240 Figura 2

